PCCP

# Promoting effect of tungsten carbide on catalytic activity of Cu for CO2 reduction

| | |
|---|---|
| Journal: | *Physical Chemistry Chemical Physics* |
| Manuscript ID | CP-ART-01-2020-000358.R2 |
| Article Type: | Paper |
| Date Submitted by the Author: | 07-May-2020 |
| Complete List of Authors: | Koverga, Andrey; Universidad Nacional de Colombia Sede Medellin<br>Florez, Elizabeth; Universidad de Medellin, Ciencias Basicas<br>Dorkis, Ludovic; Universidad Nacional de Colombia Sede Medellin<br>Rodriguez, Jose; Brookhaven National Laboratory, Chemistry Department |
| | |

# Promoting effect of tungsten carbide on catalytic activity of Cu for $CO_2$ reduction

**Andrey A. Koverga[a,b], Elizabeth Flórez[b] , Ludovic Dorkis[a] , José A. Rodriguez[c]**

[a]Universidad Nacional de Colombia sede Medellín, Facultad de Minas, Departamento de Materiales y Minerales, Grupo de Investigación en Catálisis y Nanomateriales, Medellín, Colombia

[b]Universidad de Medellín, Facultad de Ciencias Básicas, Grupo de Investigación Mat&mpac, Medellín, Colombia

[c]Chemistry Department, Brookhaven National Laboratory, Upton, NY, United States

**Abstract**

The adsorptions of H, $CO_2$, HCOO, O and CO on copper monolayer and submonolayers supported on hexagonal WC(0001) surfaces has been investigated. Calculations have been performed using density functional theory with the Perdew-Burke-Ernzerhof exchange correlation functional and D2 Van der Waals corrections. In addition, dipole corrections were also included. The catalytic properties of supported Cu on both carbon- and metal-terminated WC(0001) surfaces were explored. On carbon-terminated WC(0001) surfaces, Cu tends to be oxidized, while on the metallic terminated surface it gains charge. Results indicate that all studied Cu/WC(0001) surfaces bind all adsorbates stronger than the extended Cu(111). For CO, the binding energy is so large in some cases (1.6-2.2 eV) that it could potentially lead to a catalyst's deactivation. Nevertheless, surfaces with an adsorbed Cu monolayer, $Cu_{ML}$, are less prone to this deactivation, since there are not WC surface atoms and thus, the contribution of strong CO adsorption from the support does not play a role. Energetic barriers for HCOO formation, relative to $CO_2$ direct dissociation barriers, evidence that a hydrogen-assisted reduction path is more likely to occur on Cu/WC(0001) materials, being the $Cu_{ML}$/ metallic termination the most active system for this reaction path. On the other hand, $CO_2$ adsorption on $Cu_{ML}$ surfaces is slightly weaker on a C-terminated than on a metal-terminated surface, although both surfaces have similar dissociation barriers. This fact, together with the weaker CO adsorption on $Cu_{ML}$/C-terminated than on the metal-terminated WC(0001), suggests that the former system may be a better catalyst for $CO_2$ reduction, due to a lower surface poisoning by the $CO_2$ dissociation products. Possible deactivation of Cu/WC(0001) materials may be prevented by the introduction of hydrogen into the system, thus, promoting the formation of HCOO and avoiding CO and O formation.

## 1 Introduction

Carbon dioxide accumulation in the atmosphere is one of the important problems of modern science as rising $CO_2$ levels are estimated to have a significant impact on global climate.[1] Among proposed strategies to mitigate the effects of anthropogenic global warming is carbon sequestration. This approach is based on reducing $CO_2$ emissions via capture at a point source, with subsequent sequestration.[2,3] However, an

efficient way to utilize captured $CO_2$, such as conversion to either fuels, or carbon-based chemical materials is still required.[4-6]

Precious metals can be used to facilitate $CO_2$ conversion by hydrogen.[7,8] The main and universal disadvantage of using noble metals in chemical processes is their scarcity and high price. Thus, optimally, a non-expensive material with comparable catalytic characteristics must be found to make $CO_2$ reduction economically viable. Copper has a low cost and is an active material for the electroreduction of $CO_2$,[9,10] however its activity as thermal gas-solid catalyst still needs to be improved.

In the most common applications, heterogeneous catalysts which contain copper are generated by dispersing this element on oxides of different types,[11,12] simultaneously increasing the active area of the catalyst upon dispersion. On the other hand, carbides materials can be good candidates to be used as supports, since through the modification of electronic properties the catalytic activity of supported metals may be enhanced.[13,14] For instance, Au/TiC and Cu/TiC have been reported to be very active for $CO_2$ activation and methanol synthesis.[15]

Transition metals carbides (TMC), having catalytic activity similar or superior to the catalytic activity of platinum,[16] have been drawing attention as perspective materials for heterogeneous catalysis.[17-22] TMCs have the ability to capture, storage and activate $CO_2$ [23-25] with its further conversion to carbon-based chemical materials,[26-29] but their properties must be adjusted to improve their catalytic performance. A way to reach this goal could be by adsorbing another metal at submonolayer or monolayer levels.

Materials comprised of copper supported on TMCs have often demonstrated superior activity for $CO_2$ reduction relative to that of their components. In the case of Cu and Au adatoms on TiC, for example, a reported activity trend for methanol formation is Cu/TiC(001) >Au/TiC(001) >Cu/ZnO(001) >Cu(111), in agreement with the $CO_2$ adsorption energy trend on these surfaces.[30] Good activity for $CO_2$ activation has been also demonstrated for (001) surfaces of various TMCs.[31,32]

In the case of Cu/WC surfaces, an experimental work by Dubois, Sayama and Arakawa reported a poor catalytic performance for $CO_2$ reduction.[33] In contrast, detailed computational studies by Wannakao *et al.* on the W-terminated WC(0001) surface, decorated with Mn, Fe, Co, Ni, Cu, Zn, Ru, Rh, Pd, Ag, Ir, Pt and Au monolayers,[34,35] predicted that Me/WC systems can be active catalysts for the $CO_2$ electrochemical reduction. Although the exact origin on these discrepancies is unknown, it is important to note that while the work of Wannakao *et al.* focused on the electrocatalytic $CO_2$ reduction on W-terminated WC(0001) surface, Dubois, Sayama and Arakawa discussed the catalytic activity of a real Cu/WC system in gas phase, in which the Cu coverage and atom termination of the support were not known, which could explain the apparent contradiction. Furthermore, differences in the catalytic performance of theoretically modeled systems and real surfaces often stem from the fact that a model represents an ideal material, without

irregularities in its crystalline structure, while the structure of a real catalyst is more random and may include various surface impurities.

Nonetheless a theoretical approach is well-prepared to accurately predict catalytic properties of a material for a selected chemical process, and can be successfully employed to analyze the causes behind changes in activity of composite surfaces with respect to that of isolated parent materials. In this sense, theoretical studies have shown that copper surfaces typically catalyze hydrogen-assisted $CO_2$ reduction,[27,36,37,38] with formate (HCOO) as one of the key intermediates in methanol synthesis on pristine[27] and supported copper.[31] In contrast, direct $CO_2$ dissociation on pure Cu(111) is negligible, mainly because the extremely weak $CO_2$-Cu interactions reduce the ability of the surface to host reactions that involve a transformation of carbon dioxide on the surface.[27,39,40,41] Therefore, dispersing Cu materials on strongly $CO_2$ adsorbing supports could be a suitable strategy for improving the $CO_2$ catalytic properties of Cu surfaces, through a careful tuning of the $CO_2$ adsorption energy.

In agreement, theoretical studies have also reported an impact of the support on the electronic structure of Cu on WC[35,42] and TiC[15] and $Mo_2C$[43], which in turn may lead to changes in $CO_2$ adsorption properties on Cu/WC(0001) surfaces, and alter its activity towards C—O bond scission. Indeed, Posada-Perez *et al.*,[31] and Wannakao *et al*. [34,35] reported that $CO_2$ dissociation is possible on Cu/$Mo_2C$ and $Cu_{ML}$/W-terminated WC(0001) surfaces, respectively In this last case, however, neither the role of Cu coverage, nor the catalytic activity of carbon-terminated atoms toward $CO_2$ reduction on TM/WC(0001) materials were discussed,[34,35] and still requires clarification. Moreover, the activity of Cu/WC(0001) surfaces toward the hydrogen-assisted $CO_2$ reduction route, the common reduction path on pure Cu surfaces, with HCOO as initial intermediate during $CO_2$ hydrogenation, remains unclear.

In this sense, the present work aims to determine $CO_2$ dissociation, and adsorption properties of possible intermediate products, such as CO and O, on Cu/WC(0001), as a first step to assess the catalytic properties for $CO_2$ reduction of these materials through direct dissociation. For this, it is important to consider copper supported on both carbon- and metal- polar terminations of WC(0001), and the interaction of these Cu/WC(0001) systems with $CO_2$ and selected possible intermediates. This information can be used to compare the catalytic activity of these systems with that of pristine copper and copper supported on a similar materials, such as molybdenum carbide, and evaluate the probability for the hydrogen-assisted reduction path to occur, by analyzing the energetic barrier for HCOO formation from H and $CO_2$, and adsorption energies of HCOO on $Cu_{ML}$/WC(0001).

## 2 Computational details

Calculations have been carried out using Vienna *ab initio* simulation package (VASP).[44-47] The Projector Augmented Wave core potentials [48] as implemented by Kresse and Joubert [49] and Perdew-Burke-Ernezerhof approximation [50] to the exchange-correlation energy were used. For all the systems investigated, the D2 scheme for van der Waals corrections was applied.[51] Dipole corrections were also introduced to prevent the effect of dipole interactions between repeating images. Geometry optimization calculations were performed using the cutoff for the plane-wave basis set of 415 eV. The reciprocal space for all surfaces was approximated by a sum of *k*-points selected using 3×3×1 Monkhorst-Pack scheme[52] for the geometry optimization calculations, and 11×11×1 for the Density of States calculations.[52] The Fermi level was smeared using the Methfessel-Paxton approach [53] with a Gaussian width of smearing of 0.2 eV.

WC hexagonal phase was considered in this study as the support for Cu, specifically the (0001) surface and its C- and W- polar terminations. Pristine C-terminated and W-terminated WC(0001) surfaces, in this work denoted as C-WC(0001) and W-WC(0001), respectively, were modeled using (3×3) supercells. Each supercell was comprised of two tungsten and two carbon alternating atomic layers. To each cell a vacuum region on 15Å was added to avoid interactions between repeating images in *z* direction.

A copper monolayer was modeled by completely covering the support with Cu atoms, therefore, 9 atoms were present in $Cu_{Ml}$/WC(0001) systems, and no direct interaction of the support with adsorbed moieties took place. The submonolayer system was represented by a copper coverage of 4/9, which is an intermediate value between pristine Cu and completely covered WC(0001). This surface was denoted as $Cu_4$/ WC(0001). This coverage assures that supported Cu particles leave sufficient amount of exposed WC sites, located both in its vicinity, and far enough to evaluate the effect of these sites on CO and $CO_2$ adsorption properties in Cu/WC(0001) systems.

Structure optimization calculations have been conducted as follows: 2 out of 4 total atom layers of the support were allowed to relax simultaneously, while 2 remaining layers were frozen in a bulk-like geometry. Cu monolayer and $Cu_4$ submonolayer were allowed to relax in all three directions, together with adsorbate moieties. To verify the sufficiency of this model, adsorption energies of a single Cu atom on both terminations of the carbide were compared by using four and five layers of the support. For C-WC(0001) (W-WC(0001)) surface the adsorption energies were -4.52 (-4.05) and -4.54 (-4.07) eV for four and five layers, respectively. Close calculated values for these surfaces assured the adequacy of selected models.

The cohesion energy of the gas phase of $Cu_n$ particles was obtained from the expression

$$E_{coh} = \frac{E_{Cu_n} - nE_{Cu}}{n} \qquad \text{Eq. 1}$$

Here $E_{Cu_n}$ and $E_{Cu}$ are the energies of isolated $Cu_n$ particle and isolated Cu atom, respectively; n – is the number of Cu atoms in the particle.

Adsorption energies for Cu monolayer, $Cu_{ML}$, and Cu submonolayer, $Cu_4$, were calculated as:

$$E_{Ads}^{Cu} = E_{Cu_n + WC} - E_{Cu_n} - E_{WC} \quad \text{Eq. 2}$$

where $E_{Cu_n + WC}$ is the total energy of system with copper placed on the WC(0001) surface, $E_{Cu_n}$ – the energy of the isolated Cu atoms in vacuum, and $E_{WC}$ the energy of pristine (0001) surface. The adsorption energy per-atom can be calculated by dividing $E_{ads}$ by the number of Cu on WC(0001) surfaces.

Adsorption energies for CO and $CO_2$ on $Cu_{ML}$/WC(0001) and $Cu_4$/WC(0001) surfaces were obtained from equation 3.

$$E_{Ads} = E_{Tot} - E_{Surf} - E_{Ad} \quad \text{Eq. 3}$$

where $E_{Tot}$, $E_{Surf}$ and $E_{Ad}$ are the energies of the system with the adsorbate, of the pristine surface, and of the isolated adsorbate in vacuum, respectively. Adhesion energies of $Cu_4$ and $Cu_{ML}$ on WC(0001) surfaces can be calculated by using $E_{Ads}$:

$$E_{Adh} = E_{Ads} - \Delta E_{Surf} - \Delta E_{Cu_n} \quad \text{Eq. 4}$$

$\Delta E_{Surf}$ here is the difference between the energy of the surface with the geometry adopted upon $Cu_n$ adsorption, and of the isolated surface with relaxed geometry; $\Delta E_{Cu_n}$ is the difference between the energy of isolated $Cu_n$ structure frozen in the geometry it adopts upon adsorption, and the energy of the $Cu_n$ structure after relaxation in gas phase.

For $Cu_{ML}$/WC(0001) systems the degree of strain can be evaluated from equation 5.

$$\frac{d_{Cu-Cu(ML)} - d_{Cu-Cu(Bulk)}}{d_{Cu-Cu(Bulk)}} \times 100\% \quad \text{Eq. 5}$$

$d_{Cu-Cu(ML)}$ and $d_{Cu-Cu(Bulk)}$ are the average Cu-Cu distance in the monolayer and in bulk respectively. From this formalism, positive values would indicate expansion, while negative – contraction of the structure relative to the bulk geometry.

Cu/WC(0001) systems were further analyzed by means of Bader charge analysis,[54] as implemented in VASP by Henkelman, Arnaldsson and Hannes.[55] Having these data, it is possible to calculate charge density difference from the expression

$$\Delta\rho = \rho_{Surf+Cu_{ML/4}+Ads} - \rho_{Surf+Cu_{ML/4}} - \rho_{Ads} \quad \text{Eq. 6}$$

$\rho_{Surf+Cu_{ML/4}+Ads}$ here is charge density in the system with adsorbate, $\rho_{Surf+Cu_{ML/4}}$and $\rho_{Ads}$ are the charge distributions of the WC(0001) surface with Cu particle on it, and of the adsorbate molecule in gas phase, respectively.

Charge distributions in studied systems are obtained under the strict conditions that they must have the same geometries as in the composite system, as described elsewhere.[56] The charge distribution difference (CDD) plot can be visualized by additional software tools like VESTA [57] or VMD [58].

For $Cu_{ML}$/WC(0001) systems top, bridge, and a set of three-fold hollow adsorption sites were considered (see Figure 1). On both terminations, three-fold hollow with no atom in sublayer (E*hcp*) can be distinguished and, depending on WC(0001) surface termination, a three-fold hollow site with either a C atom (C*hcp*) or a W atom in the sublayer (W*hcp*) is available.

As the number of exposed Cu atoms on these surfaces was 9, the total coverage was equal to 1/9 for each adsorbate. Cluster systems with four-copper atoms on hexagonal WC(0001) surfaces are characterized by a lower symmetry and, consequently, a larger number of adsorption sites is available. They can be divided into sites available on the Cu particle itself (Cu sites), and on the supporting surface (WC sites), as it is shown in Figure 2. Different types of top and bridge sites available on WC sites are distinguished by their distance to the supported copper particle.

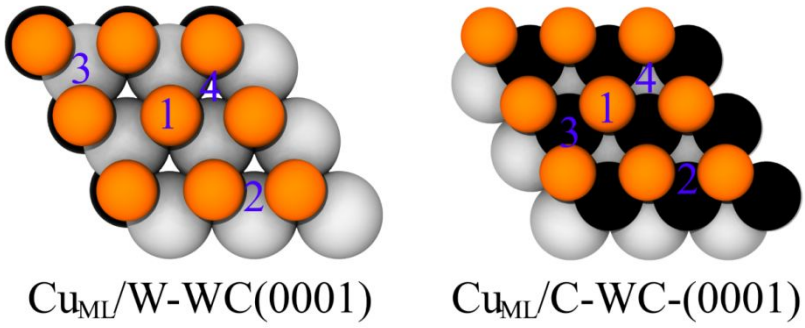


Figure 1. Adsorption sites available on $Cu_{ML}$/WC(0001) surfaces. Here tungsten, carbon and copper atoms are represented by silver, black and orange spheres, respectively. Considered sites: 1–top, 2–bridge, 3–W*hcp*/C*hcp*, 4–E*hcp*.

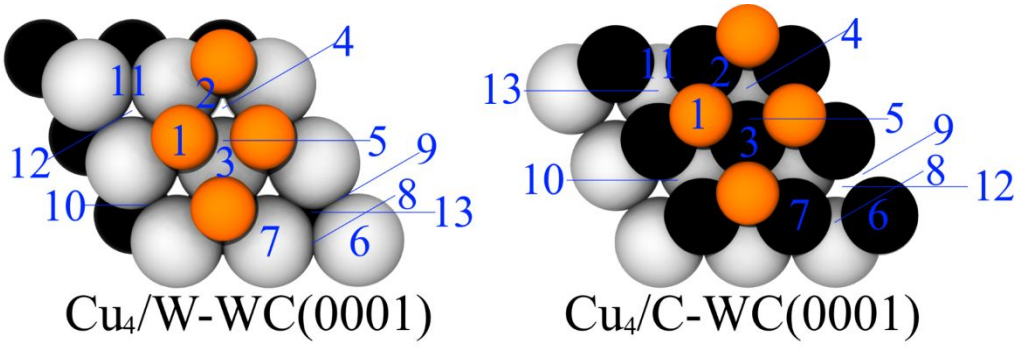


Figure 2. Adsorption sites available on $Cu_4$/WC(0001) surfaces. The colored spheres represent the same atoms as in Figure 1. Considered sites: 1–top$^{Cu}$, 2–bridge$^{Cu}$, 3–W*hcp*$^{Cu}$/C*hcp*$^{Cu}$, 4–E*hcp*$^{Cu}$, 5–4-fold$^{Cu}$, 6–top-1$^{WC}$, 7–top-2$^{WC}$, 8 – bridge-1$^{WC}$, 9–bridge-2$^{WC}$, 10–bridge-3$^{WC}$, 11–bridge-4$^{WC}$, 12–E*hcp*$^{WC}$, 13–C*hcp*$^{WC}$/W*hcp*$^{WC}$.

Energy barriers for $CO_2$ dissociation were calculated using Climbing Image Nudged Elastic Band (CI-NEB) method as implemented by Henkelman, Uberuaga and Jónsson,[59] and Henkelman and Jónsson [60].

Geometries corresponding to the most stable adsorption were used as initial images for these calculations, and final geometries were obtained by estimating preferred adsorption sites for dissociation products. The condition that total forces must be smaller than 0.01 eV/Å was used as convergence criterion. Energy barrier values, $E_b$, were calculated from the equation 7,

$$E_b = E_{TS} - E_{Ads^*} \quad \text{Eq. 7}$$

$E_{TS}$ here is the total energy of a transition state, and $E_{Ads^*}$ is the total energy of an initial state. Therefore, reported dissociation barriers were positive. Additionally, obtained transition state geometries were verified by a vibrational frequency analysis. For this, Cu and WC atoms were frozen while adsorbates were allowed to move in all three directions, and the transition state was confirmed by checking for the existence of a single imaginary frequency.

## 3 Results and discussion

### *3.1 $Cu_{ML}$ and $Cu_4$ interactions with WC(0001)*

Preferred adsorption sites for Cu on C-WC(0001) and W-WC(0001) were established by placing a single copper atom on the adsorption sites for these surfaces.[32] [26] In agreement with previously reported results,[34,35] copper was found to preferably adsorb on *hcp* sites. Specifically, on the C-WC(0001) surface, Cu occupies an *hcp* site with no atom in the sublayer (E*hcp*), whereas on W-WC(0001) surface Cu atom adsorbs on *hcp* site with C atom directly underneath (C*hcp*) (see Table 1).

Table 1. Adsorption energies for Cu atom on WC(0001) surfaces. Distances between the surface plane and Cu atoms are indicated as well. The most stable sites are hinted by bold font.

| Surface | Initial site | Final site | d (Cu-WC) / A˚ | Eads / eV |
|---|---|---|---|---|
| C-WC(0001) | Top | Top | 1.80 | -3.06 |
| | Bridge | Ehcp | 1.95 | -4.52 |
| | **Ehcp** | **Ehcp** | **1.95** | **-4.52** |
| | Whcp | Whcp | 2.05 | -4.13 |
| W-WC(0001) | Top | Top | 2.33 | -3.24 |
| | Bridge | Chcp | 2.58 | -4.05 |
| | Ehcp | Ehcp | 2.58 | -3.95 |
| | **Chcp** | **Chcp** | **2.58** | **-4.05** |

On the other hand, from Table 1 it is seen that a Cu atom initially placed on a bridge site on both C-and W-terminated surfaces shifts to an *hcp* site after relaxation (final state). Since final adsorption energies in both cases are the same as the one of a Cu atom initially placed on an *hcp* site, E*hcp* and C*hcp*, respectively, and the distance from the surface is also the same in both cases, it can be said that Cu adsorption over bridge sites on neither of the surfaces is stable.

For each WC(0001) termination, the configuration with two Cu atoms can be obtained by placing the first Cu atom on the most stable site, as summarized in Table 1, and the second atom on the remaining available sites, relaxing the geometry of the resulting systems, and selecting the one with the lowest total energy. By sequentially adding Cu atoms, and evaluating total energies of resulting systems, the structures of the $Cu_4$ cluster on WC(0001) surfaces were obtained.

Final stable configurations for $Cu_4$/ WC(0001) are given in Figure 2. These configurations are similar to the ones obtained by Posada-Pérez *et al*.,[43] where a rhombus-like geometry was reported for a $Cu_4$ cluster on molybdenum carbide. It should be noted that this flat rhombus-shaped configuration is energetically more favorable than a 3D tetrahedron-like structure for both terminations of the support. Therefore, it would be expected that small Cu clusters would wet the carbide substrate rather than forming 3D structures.

To further verify our findings, cohesion energies for this rhombus-like structure in the gas phase were also calculated. A value of -1.61 eV was obtained, close to -1.57 eV reported before for a $Mo_2C$ support.[43] Moreover, the nine Cu atoms cluster is more stable compared to four particle cluster, evidenced from the lower cohesion energy calculated for the monolayer system, -2.26 eV.

The structure of Cu monolayer supported on both terminations was obtained in a similar way, *i.e.* by sequentially occupying all available *hcp* sites with copper atoms. As it can be seen in Figure 1, resulting structures bear a resemblance to a somewhat strained Cu(111) surface. Table 2 resumes adsorption and adhesion energies, the degree of strain of Cu structures, and total net charge on copper structure. It can be seen that Cu adsorption on both terminations is exothermic, being stronger on C-WC(0001).

Table 2. Adsorption energy ($E_{ads}$), average Cu–nearest WC atom distance (d(Cu-WC)), average shortest Cu–WC surface distance (d⊥(Cu-WC)), adhesion energy ($E_{adh}$) per atom, degree of strain and charge transfer ($_{\Delta}Q$) for optimized $Cu_4$ and $Cu_{ML}$ structures on WC(0001) terminations

| nCu and WC termination | $E_{ads}$ (eV) | d(Cu-WC) (A)° [a] | d⊥(Cu-WC) (A)° [a] | $E_{adh}$ (eV) | Strain [b] % | ΔQ (*e*) |
|---|---|---|---|---|---|---|
| 4 on C-WC(0001) | -2.88 | 1.96 | 1.00 | -3.72 | – | +2.20 |
| 4 on W-WC(0001) | -2.46 | 2.56 | 1.98 | -2.68 | – | -0.71 |
| ∞ on C-WC(0001) | -2.27 | 2.04 | 1.14 | -2.63 | +13.3 | +4.04 |
| ∞ on W-WC(0001) | -1.97 | 2.65 | 2.05 | -2.05 | +11.3 | -1.48 |

[a] d corresponds to the distance between the adsorbate and the closest surface atom; d⊥ is the shortest normal distance from the adsorbate to the surface plane.

[b] Positive values correspond to expansion process.

From Table 2, it is evident that Cu-WC distances in these systems strongly depend on the surface termination. On C-WC(0001) surface, copper atoms are at a distance of ~1Å, while on the metallic termination Cu is found at a (much) larger distance, ~2 Å, which is similar to the previously reported

distances for these systems.[42] It is important to note that both of these values can be regarded practically constant as the number of Cu atoms supported on the WC(0001) increases on each surface.

For the $Cu_4$/W-WC(0001) system, calculated adhesion energy does not significantly differ from adsorption energy (Table 2), indicating that the surface and cluster deformations are not dominant. However, the adsorption of the four atom cluster on C-WC(0001) is accompanied by a significant deformation of both the cluster and the surface, evidenced by the differences between $E_{adh}$ and $E_{ads}$. In contrast, adhesion energies for both monolayer systems are quite close to the adsorption energies, suggesting a low surface and copper layer deformation upon adsorption due to the higher packing density of Cu atoms on the surface. Similarly to copper supported on orthorhombic molybdenum carbide,[43] adhesion energies decrease with the growing number of atoms of Cu available on both terminations of the support.

In the monolayer system, Cu-Cu distances are larger than those in bulk Cu, evidenced by positive strain degrees (Table 2). This expansion of Cu atoms supported on WC(0001) can be explained by the large distance between WC(0001) hollow sites on both terminations, the preferred locations for Cu atom.

In general, systems' properties with Cu particles supported on different terminations of hexagonal WC(0001) are quite close. One significant difference though is the charge distribution, clearly affected by the presence of carbon atoms on the surface (Figure S1). When $Cu_4$ and $Cu_{ML}$ are supported on C-WC(0001), there is a charge transfer from the particle to the support, *i.e.* Cu atoms on the surface acquire a net positive charge, while supporting carbon atoms get an negative charge. Contrarily, on W-WC(0001)Cu atoms get reduced, because of a charge transfer from tungsten atoms of the support to Cu atoms. This phenomenon is observed because on pristine W-WC(0001) the charge transfer takes place from metal atoms to carbon, "against" the *z* direction.[32] Consequently the dipole moment is aligned along the positive *z* direction. Thus, when a Cu particle is deposited on the surface with exposed W atoms, there is a charge transfer in *z* direction, *i.e.* from W to Cu, to compensate for the surface dipole. An exactly opposite process takes place when Cu is deposited on the C-termination.

The effect of the support termination can be also established by analyzing electron localization function (ELF) plots for the system (Figure S2). These plots evidence the existence of a higher concentration of electrons around a Cu particle on Cu/W- than on Cu/C-WC(0001). This interaction of exposed atoms of the support with adsorbed copper has a localized, non-covalent nature, more noticeable for the W- termination. A support-adsorbate charge transfer as function of the termination of the support has been also reported for Cu adsorbed on molybdenum carbide,[43] and points to a different chemical reactivity of copper depending on the termination of the support.

In agreement, a shift in the Cu density of states is also observed for monolayer and submonolayer systems on the normalized d-projected densities of state (PDOS) plots for copper presented in Figure 3,

giving a further idea on the impact of the termination of the support on the electronic properties of the adsorbate. To quantify this impact, an analysis of the d-band center position has been conducted, since the d-band center of surface atoms is one key parameter driving surface adsorption properties,[61,62] According to the d-band model,[61] a shift of the d-band center toward the Fermi level (upshift) would lead to a lower occupation of anti-bonding states in the adsorbate-surface interaction, increasing its strength, while a shift away from the Fermi level (downshift), would weaken the adsorbate-surface interaction. This correlation can be used to predict changes on materials' catalytic properties relative to the reference system. In this sense, considering the weak $CO_2$ adsorption on Cu(111)[27,39,40,41], a downshift of the d-band center would weaken the adsorption of reaction intermediates and reduce the catalytic activity, while an upshift would strengthen the adsorption, and increase the catalytic activity.

The d-band centers for Cu adatoms were calculated for all studied systems and values are given in Figure 3. From these data, downward shifts (0.07 for $Cu_{ML}$ particle and 0.11 eV – for $Cu_4$ particle) are observed for Cu/C-WC(0001) systems, with respect to the d-band center of Cu(111), -2.52 eV. Therefore, it is expected that on these surfaces adsorption of reaction intermediates during $CO_2$ reduction would be less stable than on pristine Cu(111). At first glance, this result would indicate a lower activity of these systems towards $CO_2$ reduction than the one of Cu(111), because of a weaker $CO_2$ adsorption. However , it is important to take also into account other factors that may impact the stability of intermediates on the metal overlayers, such as the degree of strain, which reduces overall coordination of supported Cu atoms, and the distance between the WC(0001) support and the supported Cu, to be able to draw a general conclusion.

In contrast, analysis of changes in the d-band center of Cu/W-WC(0001) systems evidences a upshift of Cu PDOS with respect to the position on Cu(111),, especially in the $Cu_{ML}$/W-WC(0001) system (0.14 eV) relative to the $Cu_4$/W-WC(0001) surface (0.08 eV) –. This positive upshift indicates a stronger adsorption of $CO_2$, and reduction reaction intermediates and, possibly, overall lowering of energy barriers of the processes involved in $CO_2$ reduction.

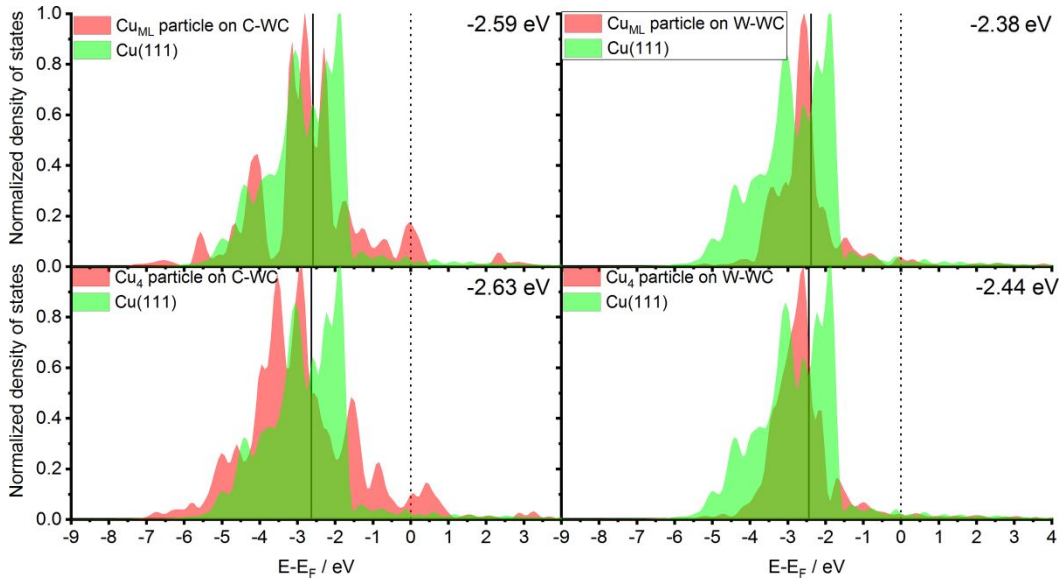


Figure 3. Normalized d-projected densities of states (PDOS) of Cu monolayers and submonolayers supported on W- and C-terminated WC(0001). For each system, the Fermi level (dashed line) and the d-band center (solid line) are indicated.

In summary, changes in the electronic structure, charge distribution and geometry of copper with the termination of the WC(0001) support opens a possibility to tune the reactivity of supported particles, depending on the reaction of interest. However a reliable knowledge on how the termination of the support impacts the interactions of Cu and possible reaction intermediates, ($CO_2$ and CO, for instance), is also required, in order to extract a conclusive picture.

### *3.2 Adsorption of CO, O, H, HCOO and $CO_2$ on $Cu_{ML}$/WC(0001) and $Cu_4$/WC(0001)*

To estimate the possibility of $CO_2$ dissociation on Cu/WC(0001), it is important to know the preferable adsorption locations and energies of the reagents, intermediates and reaction products on the surfaces. Additionally, assessing the stability of the products would help to evaluate the probability for surface deactivation, specifically in the case of direct dissociation, since CO molecule is usually very stable, and does not undergo further dissociation.

On copper surfaces, the hydrogenation agent in elementary reaction steps of chemical reduction is adsorbed atomic hydrogen, formed through $H_2$ dissociation.[63] Since the energy barrier for $H_2$ dissociation on Cu(111) is 0.52 eV,[63] it is relatively small compared to energy barriers for other steps in $CO_2$ reduction, and so, dissociation of $H_2$ was not considered in this study. Instead, only interactions of atomic H with the Cu/WC(0001) system and coadsorbed $CO_2$ were analyzed. Similarly, $CO_2$ hydrogenation on $Cu_4$/WC(0001) surfaces was not discussed in this work either. This is because in these systems, the preferred adsorption sites for $CO_2$ and H are located too close to each other and, upon coadsorption, $CO_2$ and H give rise to a significant deformation of the Cu cluster, which leads to a direct interaction of $CO_2$

with the support and its consequent activation *i.e.* to a significant shift from linear to bent geometry within the adsorbate. [24,32]

Adsorption of reagents, namely $CO_2$ and atomic H on $Cu_{ML}$/WC(0001) surfaces were analyzed to define initial images for CI-NEB calculations of both H-assisted, and direct $CO_2$ reduction routes. To estimate the probability of C – O scission, $CO_2$ adsorption on both Cu and WC sites on $Cu_4$/WC(0001) systems was considered as well. It has been reported, that $CO_2$ adsorption energies on TMC follow the same trend as their chemical activity, *i.e.* $Mo_2C > MoC > TiC >> Cu$,[30] and thus, surface reactivity can be initially assessed by analyzing $CO_2$ adsorption energies and geometries. Additionally, adsorption of the products of direct $CO_2$ dissociation was also studied, including the exposed sites of the support in $Cu_4$/WC(0001) systems, while formate adsorption was considered only on $Cu_{ML}$/WC(0001) surfaces. In all cases, interaction of $CO_2$, H, HCOO, O and CO with the Cu(111) surface was analyzed as well, to verify the accuracy of the employed model.

For atomic oxygen adsorption on Cu(111) previously reported energies, obtained using models of different precision, vary greatly from -4.99[64] to -4.31 eV.[65] The $E_{ads}$ value calculated in this work of -4.66 eV is more in line with the work of Hao *et al.*[66] where at the similar coverage adsorption energy -4.77 eV is reported. Despite these differences, the majority of published studies agree that the most energetically favored O adsorption configuration on Cu(111) is where oxygen occupies fcc site (E*hcp* in the notation of the present work). Similarly, on Cu/WC(0001), regardless of the coverage, oxygen occupies available *hcp* sites (Table 3). Compared to adsorption on Cu(111), O atoms on $Cu_{ML}$/W(0001) are additionally stabilized by the presence of the support, and the stabilization effect of the W-termination is significantly higher than for the C-termination, based on adsorption energies of -5.50 vs. -4.93 eV. As reported before, O adsorption on the WC(0001) support is very strong, ca. -7.66 eV[67].

Regarding CO, the molecule was initially placed on the adsorption sites of Cu/WC(0001) systems in a slightly tilted geometry, with the carbon atom of the adsorbate moiety directed towards the surface, as reported in previous works on CO interactions with metals and metal-terminated surfaces.[56,67,68,69] Adsorption energies on preferred adsorption sites can be seen in Table 3. Additionally, Table S1 provides adsorption energy values on all the adsorption sites considered, and Figure S3 summarizes the most stable geometries of the CO molecule on Cu/WC(0001) surfaces.

Analysis of CO adsorption on pristine Cu(111) yielded an adsorption energy of -1.16 eV for the most stable CO bonding geometry. This value is somewhat larger than the one obtained using the DACAPO package (-0.91 eV),[65] and slightly smaller than the one predicted from calculations using the CRYSTAL2003 code (-1.31).[70] Nevertheless, despite differences in adsorption energies, originating mainly from different values on calculations' parameters, such as pseudopotentials, unit cell size and plane wave cut-off energies, geometrical characteristics for the CO molecule on E*hcp* site of the Cu(111) surface, such

as the C-O bond length, and distance between the molecule and surface, are in excellent agreement with those reported in refs. 65 and 70.From data in Table 3, it is evident that on all Cu/WC(0001) systems the CO molecule is stable and adopts an almost perpendicular orientation towards the surfaces with no significant departure from the gas phase geometry. In all cases, CO adsorbs stronger than on Cu(111), regardless the termination of the support, probably due to the slightly lower coordination of surface Cu atoms relative to the one in densely packed Cu(111).

Nevertheless, while on $Cu_{ML}$ the CO adsorption is stronger on the W- (-1.72 eV) relative to the C-terminated (-1.28 eV) surface, on $Cu_4$ it appears that this trend is inverted. On $Cu_{ML}$/W-WC(0001), the trend appears because besides a lower coordination, CO adsorption is additionally promoted due to two complementary effects: the Cu d-band center upshift (Figure 3), and the surplus of charge available on the supported particle (Table 2). Indeed, comparing total net charges of CO on $Cu_{ML}$/C-WC(0001) (-0.14 *e*) and on $Cu_{ML}$/W-WC(0001) (-0.40 *e*), it is easy to see the correlation between the ability of the surface to donate the charge, and the stability of the adsorbate on this surface.

In contrast, on $Cu_4$ systems, a stronger CO adsorption on the C- (-2.15 eV) compared to W-terminated (-1.35 eV) surface is a consequence of the higher mobility of Cu atoms in $Cu_4$/C- than in W-WC(0001). This increased mobility facilitates the deformation of the cluster of Cu atoms to better accommodate the CO molecule, as depicted in Figure S3, resulting in the lower adsorption energy values. Because of this, the CO initially placed on an C*hcp* site of the Cu particle on $Cu_4$/C-WC(0001) surface, displaces the Cu adatoms, and preferably interacts with the C atom of the support, significantly distorting the rhombus-like geometry of the Cu submonolayer (Figure S3). Strong interaction with the support is confirmed by a significant elongation of the C—O bond to 1.26Å.

On the other hand, in $Cu_4$/WC(0001) systems with exposed WC sites, CO molecule preferably occupies them first, since CO adsorption on WC(0001) is more stable than on Cu. The stronger adsorption of CO on WC surfaces is evidenced by the changes in its geometry, compared to the geometry of CO in the gas phase, and total net charge transferred to the adsorbate, as it can be appreciated in Table 3.

| Surface | SL | Site | $E_{ads}$ (eV) | $E_{ads,Cu}$ / $E_{ads,WC}$ (eV) | Q (*e*) |
|---|---|---|---|---|---|
| O | | | | | |
| $Cu_{ML}$/C-WC(0001) | Cu | Ehcp | -4.93 | -4.66[a]/-4.77[66] | - |
| $Cu_{ML}$/W-WC(0001) | | Whcp | -5.50 | | |
| $Cu_4$/C-WC(0001) | Cu | Chcp | -4.75 | | |

| | | | | | |
|---|---|---|---|---|---|
| | WC | Top-1 | -6.50 | - | |
| $Cu_4$/W-WC(0001) | Cu | Whcp | -5.61 | -4.66[a]/-4.77[66] | |
| | WC | Whcp | -7.46 | -7.66[67] | |
| CO | | | | | |
| $Cu_{ML}$/C-WC(0001) | Cu | Top (1.16) | -1.28 | -1.16[a]/-0.91[65] | -0.14 |
| $Cu_{ML}$/W-WC(0001) | | Ehcp (1.19) | -1.72 | | -0.40 |
| $Cu_4$/C-WC(0001) | Cu | $Top^{WC}$ (1.26) | -2.15 | -1.16[a]/-0.91[65] | -0.45 |
| | WC | W*hcp* (1.46) | -3.39 | -3.64[32] | -0.57 |
| $Cu_4$/W-WC(0001) | Cu | Top (1.16) | -1.35 | -1.16[a]/-0.91[65] | -0.13 |
| | WC | Bridge-4 (1.24) | -2.24 | -2.39[32]/-1.81[67] | -0.87 |
| HCOO | | | | | |
| $Cu_{ML}$/C-WC(0001) | Cu | Top-Top | -3.04 | -2.81[a]/ -2.68[27] | - |
| $Cu_{ML}$/W-WC(0001) | | Top-Top | -3.86 | | |
| H | | | | | |
| $Cu_{ML}$/C-WC(0001) | Cu | C*hcp* | -2.69 | -2.51[a]/-2.45[71]/-2.53[72] | -0.25 |
| $Cu_{ML}$/W-WC(0001) | | W*hcp* | -2.93 | | -0.29 |
| $CO_2$ | | | | | |
| $Cu_{ML}$/C-WC(0001) | Cu | Chcp (1.27) | -0.32 | -0.22[a]/-0.05[39]/-0.08[27]/-0.03[40] | -0.80 |
| $Cu_{ML}$/W-WC(0001) | | Whcp (1.29) | -0.65 | | -1.00 |
| $Cu_4$/C-WC(0001) | Cu | Bridge (1.22) | -0.37 | -0.22[a]/-0.05[39]/-0.08[27]/-0.03[40] | -0.57 |
| | WC | Top-2 (1.29) | -2.19 | -2.31[32] | -0.69 |
| $Cu_4$/W-WC(0001) | Cu | Whcp (1.30) | -0.61 | -0.22[a]/-0.05[39]/-0.08[27]/-0.03[40] | -1.03 |
| | WC | Bridge-1 (1.30) | -1.80 | -1.56[32]/-1.03[67] | -1.34 |

Table 3: Preferred site, its location (SL), adsorption energies on Cu/WC ($E_{ads}$) and corresponding pristine surface ($E_{ads,Cu}$ / $E_{ads,WC}$), and Bader charge for reagents and products of $CO_2$ reduction. For CO and $CO_2$ the C—O bond length in Å is indicated in parentheses next to the stable site.

[a] Calculated using parameters described in Section 2.

Overall adsorption of O and CO is very stable on all studied surfaces, therefore all systems could undergo an eventual blockage of active adsorption sites by products of $CO_2$ dissociation to CO and O in realistic conditions, which may lead to a decline of their catalytic activity. As a result, catalytic activity of $Cu_{ML}$/WC(0001) systems for this reaction is expected to be better than that of $Cu_4$/WC(0001) materials, since there are not active WC sites because of their blocking by copper in the monolayer coverage. Adsorption of CO and O on WC surfaces is even stronger than on Cu/WC(0001) systems.

Formate bonding to Cu(111) occurs through the O atoms with an adsorption energy of -2.68 eV[27]. Calculations conducted in this study indicate a similar final geometry for the HCOO moiety (i.e. $\eta^2$-O,O bonding), and an energy of adsorption of -2.81 eV, which is slightly higher than the reported value. These differences are mainly a result of the different software package used in the present study.[27] Model setup also contributes to the final value of adsorption energies, and the observed difference of 0.13 eV may also originate from the choice of the planewave cut-off and pseudopotentials.

HCOO adsorption energies on the Cu monolayer supported on WC(0001) surfaces are listed in Table 3 and illustrations of the stable geometries can be observed in Figure S4. Similarly to adsorption on pristine Cu, HCOO is interacting through its oxygen atoms with Cu atoms on both $Cu_{ML}$/C-WC(0001) and $Cu_{ML}$/W-WC(0001), adopting a top-top location. Adsorption on the other sites available on the surface was not stable, and resulted in HCOO shifting to the top-top location. Similarly to O and CO, a small stabilization of HCOO upon adsorption on the $Cu_{ML}$/C-WC(0001) is observed, while on $Cu_{ML}$/W-WC(0001) the adsorbate stabilization was significantly higher.

Calculations on atomic H adsorption on pristine Cu(111) yielded an adsorption energy for the most stable site (E*hcp*) of -2.51 eV, in good agreement with previously published data (-2.45 eV[71] and -2.53 eV[72]). H adsorption on supported copper monolayer (Table 3) takes place on *hcp* sites, and is more stable than the adsorption on Cu(111). The $Cu_{ML}$/W-WC(0001) surface stabilizes the adsorption significantly (-2.93 vs. -2.51 eV on Cu(111)), while on the C-terminated this effect is rather small (-2.69 vs. -2.51 eV). In this latter surface, the adsorption enhancement reflects the interaction between the adsorbate and the WC support, evident from a charge density difference plot (Figure S5), in which it can be appreciated that H atom gains an additional charge from the carbon atom directly underneath. On $Cu_{ML}$/W-WC(0001) surface, additionally to the H-WC interaction, the observed upshift of Cu d-band center further enhances the adsorption of H atom.

Although obtained values for H adsorption are approximately 0.2 eV more negative than the ones reported before for an analogous system,[42] the overall trend regarding the stabilization of H adsorption because of the presence of the WC(0001) support remains. Again, in this case, more negative $E_{ads}$ values present here relative to previously reported energies mainly originate from differences in the software package used in the present work, and in the pseduopotenitals available for Quantum ESPRESSO and VASP distributions.

Adsorption energies of $CO_2$ molecule on preferred adsorption sites on the studied surfaces, and the most stable geometries of $CO_2$ are given in Table 3and Figure 4, respectively. Values for $CO_2$ adsorption on other sites is available in Table S2. Calculations of $CO_2$ adsorption on Cu(111) surface have been also performed as described in Computational Details section, and an adsorption energy of -0.22 eV was obtained for the most stable site. This energy is higher than the ones reported in other works (-0.08,[27] -

0.07[39] and -0.03 eV[40]), mainly because of different choice of computational parameters. Nevertheless, similar to what is found in the present work, adsorption energy for $CO_2$ on Cu(111) in the range from -0.22 to -0.24 eV were also reported when van der Waals corrections were applied for all the systems,[73] highlighting the effect of including this correction. Nonetheless, similarly to what has been reported in all mentioned works, an analysis of the $CO_2$ distances from the model Cu(111) surface clearly indicates physisorption of the molecule.

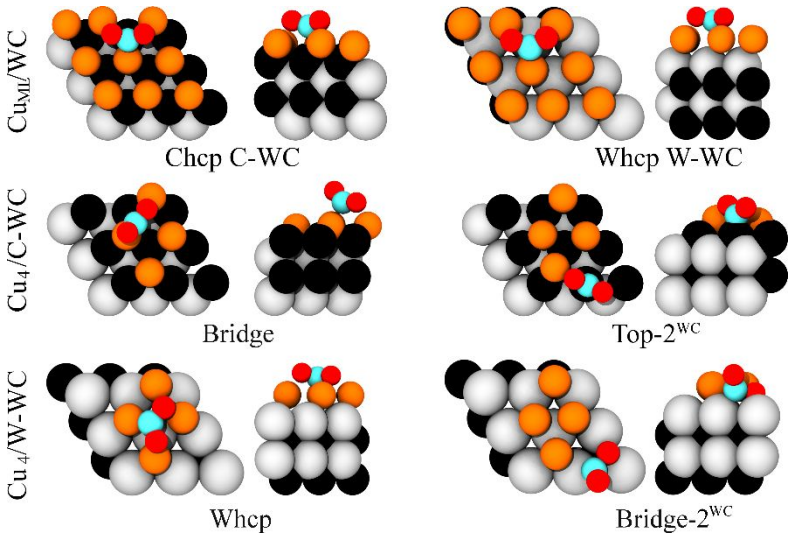


Figure 4. Top and side views of the most stable geometries for $CO_2$ after its binding on Cu/WC(0001) surfaces. The legend below each panel indicates the stable adsorption site. Sites located on the support are indicated with WC. $CO_2$ carbon atoms are represented by cyan spheres, tungsten, carbon and copper atoms are represented by silver, black and orange spheres, respectively.

When comparing adsorption of $CO_2$ on $Cu_{ML}$/WC(0001) surfaces, the role of the support termination is especially evident. Our results suggest that adsorption of $CO_2$ does not occur on most of the sites of the $Cu_{ML}$/C-WC(0001) system, except the C*hcp* site, similarly to $CO_2$ adsorption on Cu(111), where carbon dioxide weakly interacts with the surface.[27,39,40] Contrarily, on $Cu_{ML}$/W-WC(0001) surfaces, $CO_2$ adsorption is stronger and several adsorption sites can be distinguished, with W*hcp* being the most stable one (Table 3). For all stable sites in $CO_2$–$Cu_{ML}$/WC(0001) systems, a significant shift of the linear geometry of the adsorbate has been observed (see Table 3), evidencing $CO_2$ activation in these systems.[24,32] This activation has been observed on all Cu sites in Cu/WC(0001) systems, independently of the termination of the support and the copper coverage. Another common feature for all Cu sites is the orientation of $CO_2$ molecule, with its O atoms towards the surface.

Contrarily, on the $Cu_4$/C-WC(0001) system, $CO_2$ readily adsorbs, with the bridge site being the favorable one with an adsorption energy of -0.37 eV. In contrast, from all Cu sites of $Cu_4$/W-WC, only *hcp* sites are stable, W *hcp* being preferable for $CO_2$ adsorption (-0.61 eV). Nevertheless, adsorption energies of -2.19 and -1.80 eV on available WC sites on C- and W-terminated surfaces, respectively,

indicate that similarly to CO, carbon dioxide would first occupy exposed atoms of the carbide substrate, and later, populate the adsorption sites on supported Cu. Moreover, on exposed WC sites in $Cu_4$/W-WC(0001) system $CO_2$ adsorbs, in general, dissociatively, with CO occupying an available top site in the vicinity of the copper and oxygen atom adsorbing on C*hcp* site. The only two sites where $CO_2$ is stable on the surface are bridge-1 and C*hcp*, where it gets activated.

In overall, regardless the termination of the support, and the Cu coverage, $CO_2$ adsorbs stronger on Cu/WC(0001) surfaces than on pristine Cu(111), and the value of the $CO_2$ adsorption energy on Cu sites can be used as a descriptor for the surface activity towards $CO_2$ conversion to methanol, as proposed in ref. 30. Therefore, on the basis of this descriptor, the following activity trend can be predicted for all studied surfaces: $Cu_{ML}$/W-WC(0001) > $Cu_4$/W-WC(0001) > $Cu_4$/C-WC(0001) > $Cu_{ML}$/C-WC(0001) > Cu.

The observed enhanced $CO_2$ adsorption on Cu/W-WC(0001) can be attributed to the upshift of the d-band center for these surfaces, which leads to stabilization of the adsorbate.[73,74] However, from the downshift of the d-band center observed in Cu/C-WC(0001) systems (Figure 3), a deleterious effect on the strength of $CO_2$ interaction with the surface, because of the presence of the support, would have been expected. This apparent contradiction can be resolved by analyzing CDD plots for $CO_2$ – Cu/WC(0001) given in Figure 5, together with the total net charge gained by the adsorbate, summarized in Table 3. From these data, it can be seen that $CO_2$ is able to acquire a negative charge from the surface in the Cu/C-WC(0001), because of the additional involvement of the support into the charge transfer. Notice that a small depletion of charge is observed for the carbon of the WC(0001), in the layer directly underneath of Cu adatoms (See Table 2). This effect is not present in Cu/W-WC(0001) systems, and it may be seen as an additional factor stabilizing $CO_2$ molecules on Cu/C-WC(0001) surfaces.

Interestingly, the total amount of charge acquired by $CO_2$ on $Cu_4$/C-WC(0001) surface is lower than on $Cu_{ML}$/C-WC(0001), *i.e.* -0.57 vs. -0.80 *e*, respectively, while for W-terminated surfaces a comparable charge transfer to $CO_2$ has been observed for $Cu_{ML}$ and $Cu_4$, i.e. -1.00 and -1.03 *e*, respectively. This can be explained in terms of availability of supported Cu atoms for the charge transfer to $CO_2$: while in $Cu_4$/C-WC(0001) there are four Cu atoms with an initial net charge of +2.20 *e*, in $Cu_4$/W-WC(0001) Cu atoms have an initial charge of -0.71 *e* on each of them (See Table 2). Therefore in $Cu_4$/W-WC(0001) the four Cu atoms with an excessive negative net charge can provide $CO_2$ with a charge, comparable to the one on the $Cu_{ML}$/W-WC(0001) system. Contrary, on $Cu_4$/C-WC(0001) surface the copper atoms interacting with $CO_2$ are initially depleted of the charge, and are not able to give the same charge as in the case of $Cu_{ML}$.

CDD plots of $CO_2$ adsorbed on exposed sites of WC(0001) support are characterized by a significant charge transfer from WC to the adsorbate, similar to $CO_2$ adsorption on a pristine WC(0001) surface.[32] This result implies that the presence of Cu adatoms does not affect significantly the adsorption properties of WC for $CO_2$ adsorption.

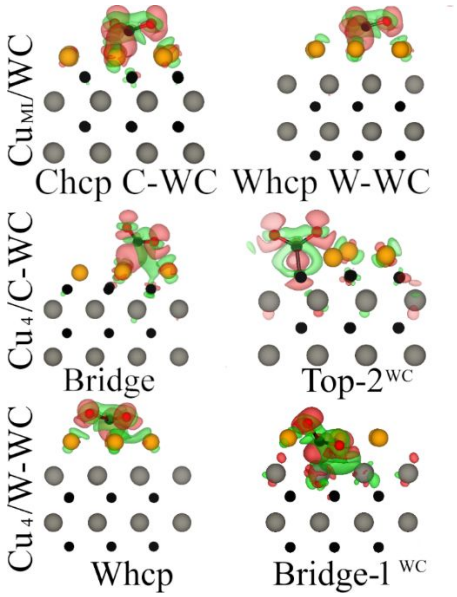


Figure 5. Charge density difference (CDD) plots for $CO_2$ adsorbed on Cu/WC(0001) surfaces. Sites located on the support are indicated with WC. Here green and red regions correspond to a charge loss (atoms become more positively charged) and charge accumulation (atoms become more negatively charged), respectively.

It is important to highlight that while on Cu/W-WC(0001) systems the $CO_2$ molecule is stabilized and activated via both O – Cu and C – Cu interactions, on Cu/C-WC(0001) systems the stabilization of the adsorbate is mainly achieved through a O – Cu interaction, revealing another distinctive effect of the support termination. This can be clearly seen in the ELF plots for $CO_2$ adsorption on Cu/WC(0001), as shown in Figure 6. From this figure, the lower probability to find an electron close to a C atom of adsorbed $CO_2$ on Cu/C-WC(0001) than on Cu/W-WC(0001) surfaces is evidenced. In agreement, note that an oxygen atom of $CO_2$ adsorbed on $Cu_{ML}$/C- gets more charge than on $Cu_{ML}$/W-WC(0001), *i.e.* -1.26 vs. -1.10 *e*, respectively, and the partial charge of the C atom of the adsorbed $CO_2$ on $Cu_{ML}$/C-WC(0001) (+1.72 *e*) is close to its value in gas phase (+1.86 *e*), while on $Cu_{ML}$/W-WC(0001) it is significantly less positive (+1.20 *e*). These two facts strongly indicate that in the $Cu_{ML}$/W-WC(0001) system interaction between the adsorbate and surface additionally takes place through C – Cu interactions.

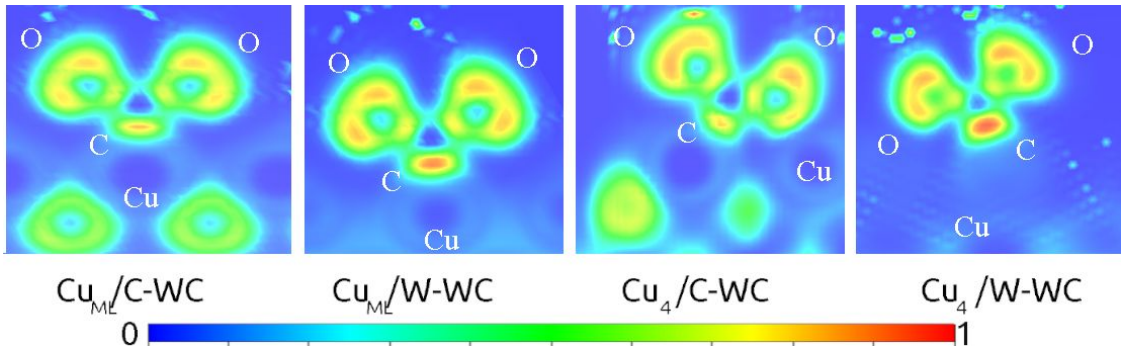


Figure 6. 2D ELF plots for $CO_2$ adsorption on studied Cu/WC(0001) surfaces, made in the plane of the $CO_2$ molecule. C, O and Cu atoms adjacent to the adsorbate are indicated. The probability of finding electron varies from 0 (blue) to 1 (red).

### *3.3 $CO_2$ reduction on $Cu_4$/WC(0001) and $Cu_{ML}$/WC(0001)*

Prior to study hydrogen-assisted $CO_2$ reduction to HCOO, it was important to assess the coadsorption of $CO_2$ and H on $Cu_{ML}$/WC(0001) and estimate its possible effect on the reactivity of the system. For this the adsorbates were placed on their most stable sites on each surface and were allowed to relax simultaneously. Adsorption energy for each moiety upon coadsorption were calculated as:

$$E_{ads,CO2(H)} = E_{Surf+CO2+H} - E_{gas,\ CO2(H)} - E_{Surf+H(CO2)} \qquad \text{Eq. 8}$$

Any change in adsorption energy of one species in the presence of the other, must be equal to the change in adsorption energy of the other, as this change gives the lateral interaction energy between $CO_2$ and H. Analysis of adsorption energies of $CO_2$ and H on Cu(111) indicates a +0.05 eV destabilization of the adsorbates upon coadsorption ($E_{ads}$ of each moiety becomes more positive). On $Cu_{ML}$/C-WC(0001), this decrease is +0.02 eV, which, taking into account the role of the $CO_2$ adsorption energy as a potential descriptor of the catalytic activity towards $CO_2$ reduction discussed above, suggests that this system should have a catalytic activity comparable to, or slightly better than, the one of pristine Cu(111). Contrarily, on $Cu_{ML}$/W-WC(0001), H and $CO_2$ coadsorption leads to an stabilization of the adsorbates by -0.06 eV ($E_{ads}$ of each moiety becomes more negative), implying that this system may show a significant improvement on the catalytic activity for $CO_2$ hydrogenation compared to Cu(111) and $Cu_{ML}$/C-WC(0001).

Once adsorption energies for coadsorption of $CO_2$ and H are known, the stable $CO_2$ and H coadsorption geometries on each surface were used as initial images to study the $CO_2 + H \rightarrow HCOO$ process, while the stable top-top HCOO geometries, depicted in Figure S4, represented the final images for the CI-NEB calculations of HCOO formation from $CO_2$ and H. Results can be seen in FiguresFigure 7 andFigure 8, where energy barriers for HCOO formation, and geometries of initial, transition and final states are summarized. The same process was also studied on Cu(111) by using the same system parameters, such as unit cell size, cut-off energy, k-points, among others, to assure the accuracy of the model, and to be able to compare consistently obtained barriers.

$CO_2$ hydrogenation to HCOO on Cu(111) typically occurs with an energy barrier of 0.86-0.87 eV[27,63] while our results indicate an energetic barrier of 0.80 eV. This difference, although not very large, may originate from a variety of factors, such as different sizes of unit cells, pseudopotentials and software packages used in this work and in the reported literature.[6327] The most important difference, however, is that D2 van der Waals corrections have been used throughout this work, while in previous studies, dedicated to $CO_2$ interaction and dissociation on Cu(111), no such corrections have been introduced into the models. Differences of ~ 0.1 eV have been reported for formic acid dehydrogenation on Pt(111) with and without van der Waals corrections,[63] consistent with what has been found here. In the case of a direct $CO_2$ dissociation, typical reported energy barriers without vdW corrections are 1.40-1.70 eV,[40,76] while by including these corrections a value of 1.33 eV[77] has been reported, also in close agreement with the value of 1.28 eV found in this work.

From Figure 7, it is evident that $Cu_{ML}$/WC has lower barriers for $CO_2$ hydrogenation compared to Cu(111): 0.74 vs.0.80 eV, and 0.65 vs. 0.80 eV for a C- and W-terminated WC(0001) support, respectively, implying an improved catalytic activity of Cu/WC(0001) surfaces with respect to pristine Cu(111). However, even the lowest energy barrier for the WC supported system, *i.e.* $Cu_{ML}$/W-WC(0001), is 0.19 eV higher than the one found for Cu/Mo-$Mo_2C$ (0.46 eV),[31] suggesting that $Mo_2C$-supported Cu would perform better as a catalyst for $CO_2$ hydrogenation than Cu/WC(0001).

The trend in the catalytic activity for $CO_2$ hydrogenation to HCOO, would be $Cu_{ML}$/W-WC(0001) > $Cu_{ML}$/C-WC(0001) > Cu(111), and it is in direct correlation with the stabilization of $CO_2$ and H upon coadsoprtion on these surfaces (-0.06 vs. +0.02 vs. +0.05 eV for $Cu_{ML}$/W-WC, $Cu_{ML}$/C-WC(0001) and Cu(111), respectively). Therefore, from comparison of the adsorption energies of $CO_2$ and H upon coadsorption on a surface, and of the stability of the individual species on the same surface, an initial assessment of the catalytic activity of a given material for $CO_2$ hydrogenation can be made, and this result could be an useful criteria to theoretically screen possible new catalytic materials.

The process of HCOO formation on $Cu_{ML}$/WC(0001) surfaces comprises the reduction of the distance between $CO_2$ and H, together with the simultaneous reorientation of the O atom of the $CO_2$ molecule towards the hydrogen atom. Calculated singular imaginary frequencies confirm that the found intermediate geometries correspond to the transition states of the $CO_2 + H \rightarrow HCOO$ process, as it is shown below each panel in Figure 8 (a). Direct $CO_2$ dissociation on Cu/WC(0001) is also characterized by lower $E_b$ values than the energy barrier for Cu(111), (0.78 and 0.67 eV for $Cu_{ML}$/C-WC(0001) and $Cu_{ML}$/W-WC, respectively). On $Cu_4$/W-WC(0001), an energy barrier of 0.74 eV is calculated. This result suggests a higher activity of $Cu_{ML}$/WC(0001) surfaces for the catalytic C–O bond cleavage (Figure 7).

On $Cu_{ML}$/WC(0001) surfaces, the transition state corresponds to the reorientation of one C–O bond, becoming perpendicular to the surface, and the elongation of the other C–O bond, caused by the movement

of the oxygen atom towards a stable hollow site, which can be appreciated in Figure 8 (b). A similar transition state of the $CO_2$ dissociation process takes also place on $Cu_4$/WC(0001). Instead, on Cu sites of $Cu_4$/C-WC(0001) a significant rearrangement of Cu atoms occurs during the $CO_2$ dissociation process, giving rise to the highest energetic barrier (0.92 eV) calculated for WC supported surfaces. For $Cu_{ML}$/WC(0001), $E_b$ values are close to those reported for $Cu_{ML}/Mo_2C$,[31] suggesting a similar reactivity of these surfaces for the $CO_2$ dissociation process. However, it is possible that Cu supported on molybdenum carbide may outperform Cu/WC(0001) systems, since the energy barrier values reported for the former system do not include van der Waals corrections. This fact highlights the importance to include this type of corrections within the calculations.

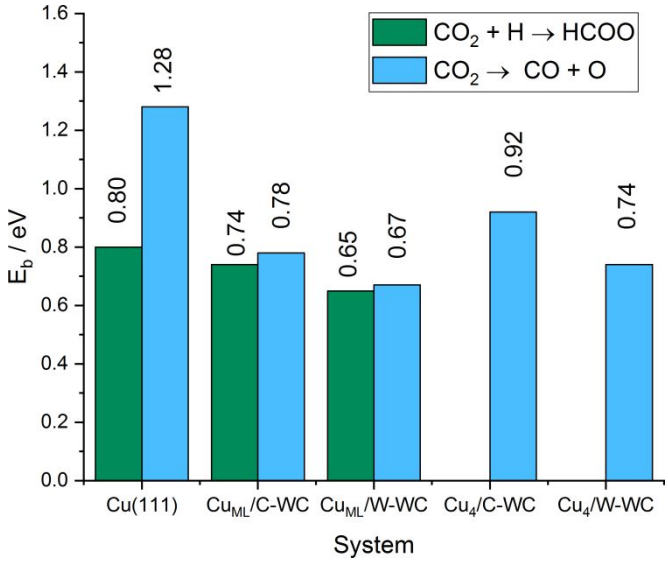


Figure 7. Energy barriers calculated for the $CO_2 + H \rightarrow HCOO$ and $CO_2 \rightarrow CO + O$ processes on Cu sites of the studied surfaces.

$CO_2$ dissociation barriers on WC sites of $Cu_4$/WC(0001) are close to calculated values on clean WC(0001) surface for equivalent terminations (0.79 vs. 0.71 eV[32], and 0.04 vs. 0.08 eV[32] for C- and W-terminated WC, respectively), suggesting a low impact of Cu on the reactivity of the carbide. In the case of $Cu_4$/W-WC(0001), the appearance of the small barrier of 0.04 eV can be attributed to $CO_2$ diffusion from the initial site toward the top-2 site, from where a barrierless dissociation takes place, a result confirmed by frequency analysis where no imaginary frequencies were found. Instead, the most obvious difference between $Cu_4$/ and pristine C-WC(0001) is that on the WC sites of $Cu_4$/C-WC(0001) the dissociation product, namely CO, is additionally stabilized by the nearby Cu adatoms (Figure S6), making the reverse process for the $CO_2$ formation more endothermic than on C-WC(0001) surface, where the dissociation products are less stable.

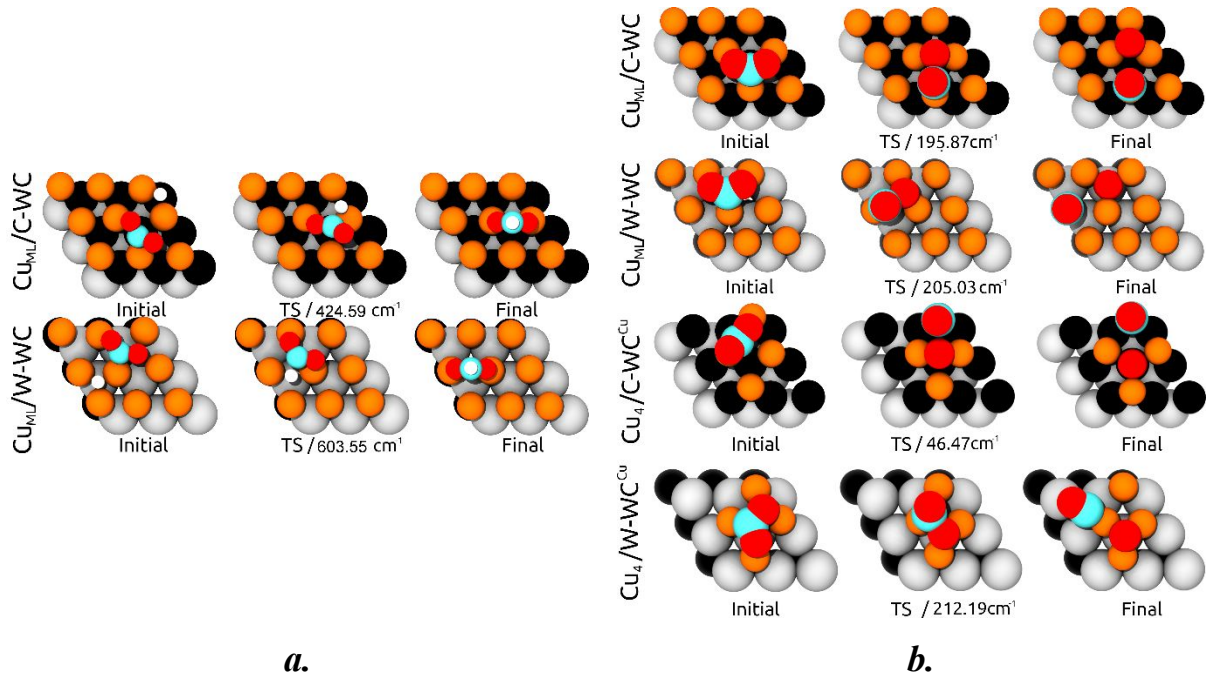


Figure 8. Initial, transition and final states geometries for hydrogen-assisted $CO_2$ dissociation (a) and direct dissociation (b) on Cu/WC(0001) surfaces. Carbon atoms of $CO_2$, HCOO and CO are represented by cyan spheres; tungsten, carbon and copper atoms are represented by silver, black and orange spheres, respectively. Vibrational frequencies are given for the TS where possible.

In summary, obtained data suggests that composite Cu/WC(0001) systems are more active for $CO_2$ reduction than a bare Cu surface due to their ability to adsorb and activate the $CO_2$ molecule. Also, energy barriers for both HCOO formation, and direct $CO_2$ dissociation on $Cu_{ML}$/WC(0001) are lower than the ones found on Cu(111), confirming an improved reactivity of Cu/WC(0001) surfaces, with the hydrogen-assisted reduction to occur more likely than direct C—O bond cleavage, regardless of the termination of the support. The biggest distinctive feature of Cu/WC(0001) surfaces is the ability to stabilize the $CO_2$ molecule on Cu sites, not achievable on bare copper surfaces.[27,39,40] The $CO_2$ coverage in Cu/WC(0001) is a function of the termination of the WC(0001) support, *i.e.* on the $Cu_{ML}$/W-WC(0001) $CO_2$ may cover the whole surface, while there is only one stable site for $CO_2$ adsorption on the $Cu_{ML}$/C-WC(0001), which in turn could result in a lower coverage.

$CO_2$ adsorption energies on Cu/$Mo_2C$ imply a better catalytic activity of Cu/WC(0001) systems than that of Cu/$Mo_2C$ for $CO_2$ reduction, since corresponding values on $Cu_{ML}$/WC(0001) (-0.06[31] vs. -0.32 eV on $Cu_{ML}$/C-TMC and -0.14[31] vs. -0.65 eV on $Cu_{ML}$/Me-TMC) are higher than on $Cu_{ML}$/$Mo_2C$. However, by taking into account the close values for $CO_2$ dissociation barriers found on Cu/WC(0001) and Cu/$Mo_2C$, and the possibility that with the van der Waals corrections the dissociation barriers on Cu/$Mo_2C$ surface would be somewhat lower, a similar catalytic performance of these two systems for $CO_2$ reduction would

be expected. On the other hand, the impact of the Cu coverage on the $CO_2$ stability is quite small. Instead, calculations suggest that it affects dissociation barriers more significantly: note that on $Cu_4$/WC(0001) dissociation barriers are consistently higher than on the $Cu_{ML}$/WC, on both terminations of the support. This effect of Cu coverage could be reflected on real systems as an effect of the Cu particle size on the reactivity of Cu/WC catalysts .

Relative to $Cu_{ML}$/WC(0001), $Cu_4$/WC(0001) systems provide additional sites, located on the carbide, for interaction with carbon dioxide.. On these WC sites, the surface reactivity is similar to $CO_2$ dissociation on pristine terminations of WC(0001) surface, implying that the impact of the support on the properties of supported Cu adatoms is greater than the effect caused by the presence of Cu atoms on the WC(0001) . In this sense, CO adsorption on WC sites is very stable, suggesting the possibility of an eventual blockage of WC-sites on these surfaces, which would leave only Cu sites available for the interaction with adsorbates. This possibility would dramatically reduce the active area of the catalyst, and would make $Cu_{ML}$/WC(0001) systems a preferable choice as a catalyst for $CO_2$ reduction. Importantly, as it was discussed above, the products of direct $CO_2$ dissociation are very stable on all the Cu/WC(0001) systems. Therefore, for practical applications, the performance of Cu/WC(0001) for $CO_2$ reduction may be optimized by assuring the presence of hydrogen in the system, and promoting the formation of HCOO intermediate while avoiding the direct $CO_2$ dissociation.

## 4 Conclusions

Periodic DFT calculations have been performed on $Cu_4$/WC(0001) and $Cu_{ML}$/WC(0001) systems to study adsorption and dissociation of $CO_2$. Results show that the structure and electronic properties of the supported copper are strongly influence by the termination of the support, *i.e.* either a carbon or a metal termination. The impact of the WC(0001) termination can be mostly seen on the d-band center shift, and the charge distribution on Cu/WC(0001) systems, which clearly demonstrates that on a C-terminated, supported Cu atoms give electrons to the support, while on W-terminated a gain of charge by Cu is observed. These changes directly impact the adsorption of $CO_2$, and products of its reduction, such as of CO, O and HCOO.

Our study shows that Cu/WC(0001) surfaces are able to stabilize and activate the $CO_2$ molecule. This may offer additional reaction routes for $CO_2$ reduction and hydrogenation, not available on pristine copper due to the a weak adsorbate-surface interaction. By using the $CO_2$ adsorption energy as a descriptor for the expected catalytic activity of the material towards $CO_2$ reduction, a higher activity of Cu/WC(0001) is suggested, compared to pristine copper and higher or similar to Cu/$Mo_2C$. Calculated energy barriers for

$CO_2$ hydrogenation to HCOO and direct dissociation processes on Cu/WC(0001) surfaces were found to be lower than on unsupported copper, confirming a higher reactivity of the WC-supported Cu. Direct $CO_2$ dissociation barriers were higher than the barriers for HCOO formation, pointing out that the hydrogenation process is energetically preferable, compared to C—O bond cleavage on these surfaces..

Overall the data shows that Cu/WC materials are expected to be better catalysts for $CO_2$ reduction, than pristine Cu(111). Even though $CO_2$ adsorption is slightly stronger on $Cu_{ML}$/W- than on $Cu_{ML}$/C-WC(0001), similar dissociation barriers, and weaker CO adsorptions on $Cu_{ML}$/C-WC(0001) suggest that this system would be a better catalyst for C—O bond scission. Similarly, a lower barrier for HCOO formation on $Cu_{ML}$/W- than on $Cu_{ML}$/C-WC(0001) implies a better catalytic activity of the former system for hydrogen-assisted $CO_2$ reduction.

In general the obtained information clearly shows an enhancing role of the support on the catalytic properties of copper, and it may be used for the further design of materials, active for $CO_2$ reduction.

**Acknowledgements**

Authors would like to thank Universidad de Medellín, UdeM, (A. Koverga and E. Florez), Facultad de Minas from Universidad Nacional de Colombia (L. Dorkis), and the U.S. Department of Energy (DOE), Office of Science, Office of Basic Energy Sciences, Division of Chemical Sciences, Biosciences and Geosciences, under contract No. DE-SC0012704 (J.A. Rodriguez), for the financial support.

## References

1 M. Pera-Titus, *Chem. Rev.*, 2014, **114**, 1413–1492.

2 H. Yang, Z. Xu, M. Fan, R. Gupta, R. B. Slimane, A. E. Bland and I. Wright, *J. Environ. Sci.*, 2008, **20**, 14–27.

3 N. MacDowell, N. Florin, A. Buchard, J. Hallett, A. Galindo, G. Jackson, C. S. Adjiman, C. K. Williams, N. Shah and P. Fennell, *Energy Environ. Sci.*, 2010, 3, 1645–1669.

4 D. J. Darensbourg, *Inorg. Chem.*, 2010, **49**, 10765–10780.

5 A. Dibenedetto, A. Angelini and P. Stufano, *J. Chem. Technol. Biotechnol.*, 2014, **89**, 334–353.

6 M. Corsten, A. Ramírez, L. Shen, J. Koornneef and A. Faaij, *Int. J. Greenh. Gas Control*, 2013, **13**, 59–71.

7 A. V. Boix, M. A. Ulla and J. O. Petunchi, *J. Catal.*, 1996, **162**, 239–249.

8 S. Alayoglu, S. K. Beaumont, F. Zheng, V. V. Pushkarev, H. Zheng, V. Iablokov, Z. Liu, J. Guo, N. Kruse and G. A. Somorjai, *Top. Catal.*, 2011, **54**, 778–785.

9 Y. Hori, K. Kikuchi and S. Suzuki, *Chem. Lett.*, 1985, **14**, 1695–1698.

10 Y. Hori, R. Takahashi, Y. Yoshinami and A. Murata, *J. Phys. Chem. B*, 1997, **101**, 7075–7081.

11 G. V. Sagar, P. V. R. Rao, C. S. Srikanth and K. V. R. Chary, *J. Phys. Chem. B*, 2006, **110**, 13881–13888.

12 R. Van Den Berg, J. Zečević, J. Sehested, S. Helveg, P. E. De Jongh and K. P. De Jong, *Catal. Today*, 2016, **272**, 87–93.

13 S. Posada-Pérez, P. J. Ramírez, J. Evans, F. Viñes, P. Liu, F. Illas and J. A. Rodriguez, *J. Am. Chem. Soc.*, 2016, **138**, 8269–8278.

14 J. A. Rodriguez, J. Evans, L. Feria, A. B. Vidal, P. Liu, K. Nakamura and F. Illas, *J. Catal.*, 2013, **307**, 162–169.

15 A. B. Vidal, L. Feria, J. Evans, Y. Takahashi, P. Liu, K. Nakamura, F. Illas and J. A. Rodriguez, *J. Phys. Chem. Lett.*, 2012, **3**, 2275–2280.

16 R. B. Levy and M. Boudart, *Science*, 1973, **181**, 547–549.

17 P. M. Patterson, T. K. Das and B. H. Davis, *Appl. Catal. A Gen.*, 2003, **251**, 449–455.

18 P. Liu and J. A. Rodriguez, *J. Phys. Chem. B*, 2006, **110**, 19418–19425.

19 N. M. Schweitzer, J. A. Schaidle, O. K. Ezekoye, X. Pan, S. Linic and L. T. Thompson, *J. Am. Chem. Soc.*, 2011, **133**, 2378–2381.

20 M. D. Porosoff, X. Yang, J. A. Boscoboinik and J. G. Chen, *Angew. Chemie - Int. Ed.*, 2014, **53**, 6705–6709.

21 L. K. Ono, D. Sudfeld and B. Roldan Cuenya, *Surf. Sci.*, 2006, **600**, 5041–5050.

22 K. Z. Qi, G. C. Wang and W. J. Zheng, *Surf. Sci.*, 2013, **614**, 53–63.

23 C. Kunkel, F. Viñes and F. Illas, *Energy Environ. Sci.*, 2016, **9**, 141–144.

24 S. Posada-Pérez, F. Viñes, P. J. Ramirez, A. B. Vidal, J. A. Rodriguez and F. Illas, *PCCP*, 2014, **16**, 14912–14921.

25 N. Li, X. Chen, W. J. Ong, D. R. Macfarlane, X. Zhao, A. K. Cheetham and C. Sun, *ACS Nano*, 2017, **11**, 10825–10833.

26 W. Leitner, *Angew. Chemie Int. Ed. English*, 1995, **34**, 2207–2221.

27 L. C. Grabow and M. Mavrikakis, *ACS Catal.*, 2011, **1**, 365–384.

28 J. Choudhury, *ChemCatChem*, 2012, 4, 609–611.

29 Y. N. Li, R. Ma, L. N. He and Z. F. Diao, *Catal. Sci. Technol.*, 2014, 4, 1498–1512.

30 S. Posada-Pérez, F. Viñes, J. A. Rodriguez and F. Illas, *Top. Catal.*, 2015, **58**, 159–173.

31 S. Posada-Pérez, P. J. Ramírez, R. A. Gutiérrez, D. J. Stacchiola, F. Viñes, P. Liu, F. Illas and J. A. Rodriguez, *Catal. Sci. Technol.*, 2016, **6**, 6766–6777.

32 A. A. Koverga, E. Flórez, L. Dorkis and J. A. Rodriguez, *J. Phys. Chem. C*, 2019, **123**, 8871–8883.

33 J.-L. Dubois, K. Sayama and H. Arakawa, Chem. Lett., 1992, 21, 5-8.

34 S. Wannakao, N. Artrith, J. Limtrakul and A. M. Kolpak, *ChemSusChem*, 2015, **8**, 2745–2751.

35 S. Wannakao, N. Artrith, J. Limtrakul and A. M. Kolpak, *J. Phys. Chem. C*, 2017, **121**, 20306–20314.

36 Y. Yang, J. Evans, J.A. Rodriguez, M.G. White, P. Liu, Phys. Chem. Chem. Phys. 12, (2010) 9909–9917.

37 P.B. Rasmussen, P.M. Holmblad, T. Askgaard, C.V. Ovesen, P. Stolze, N.K. Norskov, I. Chorkendorff, Catal. Lett. 26 (1994) 373.

38 P.A. Taylor, P.B. Rasmussen, C.V. Ovesen, I. Chorkendorff, Surf. Sci. 261 (1992) 191.

39 G. C. Wang, L. Jiang, Y. Morikawa, J. Nakamura, Z. S. Cai, Y. M. Pan and X. Z. Zhao, *Surf. Sci.*, 2004, **570**, 205–217.

40 X. Liu, L. Sun and W.-Q. Deng, *J. Phys. Chem. C*, 2018, **122**, 8306–8314.

41 H. J. Freund and M. W. Roberts, Surf. Sci. Rep., 1996, 25, 225−273.

42 D. D. Vasić Anićijević, V. M. Nikolić, M. P. Marčeta-Kaninski and I. A. Pašti, *Int. J. Hydrogen Energy*, 38 (2013) 16071-16079.

43 S. Posada-Pérez, F. Viñes, J. A. Rodríguez and F. Illas, *J. Chem. Phys.*, 2015, **143**, 114704.

44 G. Kresse and J. Hafner, *Phys. Rev. B*, 1993, **47**, 558–561.

45 G. Kresse and J. Hafner, *Phys. Rev. B*, 1994, **49**, 14251–14269.

46 G. Kresse and J. Furthmüller, *Phys. Rev. B - Condens. Matter Mater. Phys.*, 1996, **54**, 11169–11186.

47 G. Kresse and J. Furthmüller, *Comput. Mater. Sci.*, 1996, **6**, 15–50.

48 P. E. Blöchl, *Phys. Rev. B*, 1994, **50**, 17953–17979.

49 D. Joubert, *Phys. Rev. B - Condens. Matter Mater. Phys.*, 1999, **59**, 1758–1775.

50 J. P. Perdew, K. Burke and M. Ernzerhof, *Phys. Rev. Lett.*, 1996, **77**, 3865–3868.

51 S. Grimme, *J. Comput. Chem.*, 2004, **25**, 1463–1473.

52 H. J. Monkhorst and J. D. Pack, *Phys. Rev. B*, 1976, **13**, 5188–5192.

53 M. Methfessel and A. T. Paxton, *Phys. Rev. B*, 1989, **40**, 3616–3621.

54 R.F. W. Bader, Atoms in Molecules: A Quantum theory, Oxford University Press, Oxford, U.K., 1990.

55 G. Henkelman, A. Arnaldsson and H. Jónsson, *Comput. Mater. Sci.*, 2006, **36**, 354–360.

56 A. A. Koverga, S. Frank and M. T. M. Koper, *Electrochim. Acta*, 2013, **101**, 244–253.

57 K. Momma and F. Izumi, *J. Appl. Crystallogr.*, 2011, **44**, 1272–1276.

58 W. Humphrey, A. Dalke and K. Schulten, *J. Mol. Graph.*, 1996, **14**, 33–38.

59 G. Henkelman, B. P. Uberuaga and H. Jónsson, *J. Chem. Phys.*, 2000, **113**, 9901–9904.

60 G. Henkelman and H. Jónsson, *J. Chem. Phys.*, 2000, **113**, 9978–9985.

61 B. Hammer and J. K. Nørskov, Electronic Factors Determining the Reactivity of Metal Surfaces, Surf. Sci., 1995, 343, 211–220.

62 B. Hammer and J. K. Nørskov, Why Gold is the Noblest of All the Metals, Nature, 1995, 376, 238–240.

63 L. Ou, *RSC Adv., 2015*, 5, 57361-57371.

64 D. Torres, K. M. Neyman and F. Illas, *Chem. Phys. Lett.*, 2006, **429**, 86-90.

65 L. Xu, J. Lin, Y. Bai and M. Mavrikakis, *Top. Catal.*, 2018, **61**, 736–750.

66 X. Hao, R. Zhang, L. He, Z. Huang and B. Wang, *Mol. Catal.*, 2018,**445**, 152-162.

67 Y. J. Tong, S. Y. Wu and H. T. Chen, *Appl. Surf. Sci.*, 2018, **428**, 579–585.

68 M. Gajdoš, A. Eichler and J. Hafner, *J. Phys. Condens. Matter*, 2004, **16**, 1141–1164.

69 I. V. Yudanov, A. Genest, S. Schauermann, H. J. Freund and N. Rösch, *Nano Lett.*, 2012, **12**, 2134–2139.

70 M. Neef and K. Doll, *Surf. Sci.*, 2006, **600**, 1085–1092.

71 P. Ferrin, S. Kandoi, A. U. Nilekar, and M. Mavrikakis, *Surface Science*, 2012, 606(7-8), 679–689.

72 M. Luo, G. Hu, and M. Lee, *Surface Science*, 2007, 601(6), 1461–1466.

73 A.A.B. Padama, J.D. Ocon, H. Nakanishi, H. Kasai, J. Phys.: Condens. Matter , 2019 31 415201.

74 L. Ou, Y. Chen, J. Jin, RSC Adv., 2016,6, 67866-67874.

75 D. Yuan, H. Liao, W. Hu, PCCP, 2019, 21, 21049-21056.

76 O. Klaja, J. Szczygieł, J. Trawczyński and B. M. Szyja, *Theor. Chem. Acc.*, 2017, **136**, 98.

77 F. Muttaqien, Y. Hamamoto, K. Inagaki and Y. Morikawa, *J. Chem. Phys.*, 2014, **141**, 034702.